ARMY RESEARCH LABORATORY

Surface Characteristics of Etched and Non-etched Silicon Germanium (SiGe)/Si Graded Structure with Varying Ge Concentration Grown by Ultra-high Vacuum (UHV)/ Chemical Vapor Deposition (CVD) for Optoelectronic and Power Conversion Applications

by Fred Semendy, Patrick Taylor, Greg Meissner, and Priyalal Wijewarnasuriya

ARL-TR-6128 **September 2012**

Approved for public release; distribution unlimited.

NOTICES

Disclaimers

The findings in this report are not to be construed as an official Department of the Army position unless so designated by other authorized documents.

Citation of manufacturer's or trade names does not constitute an official endorsement or approval of the use thereof.

Destroy this report when it is no longer needed. Do not return it to the originator.

Army Research Laboratory
Adelphi, MD 20783-1197

ARL-TR-6128 **September 2012**

Surface Characteristics of Etched and Non-etched Silicon Germanium (SiGe)/Si Graded Structure with Varying Ge Concentration Grown by Ultra-high Vacuum (UHV)/ Chemical Vapor Deposition (CVD) for Optoelectronic and Power Conversion Applications

Fred Semendy, Patrick Taylor, Greg Meissner,
and Priyalal Wijewarnasuriya
Sensors and Electron Devices Directorate, ARL

Approved for public release; distribution unlimited.

REPORT DOCUMENTATION PAGE

Form Approved
OMB No. 0704-0188

Public reporting burden for this collection of information is estimated to average 1 hour per response, including the time for reviewing instructions, searching existing data sources, gathering and maintaining the data needed, and completing and reviewing the collection information. Send comments regarding this burden estimate or any other aspect of this collection of information, including suggestions for reducing the burden, to Department of Defense, Washington Headquarters Services, Directorate for Information Operations and Reports (0704-0188), 1215 Jefferson Davis Highway, Suite 1204, Arlington, VA 22202-4302. Respondents should be aware that notwithstanding any other provision of law, no person shall be subject to any penalty for failing to comply with a collection of information if it does not display a currently valid OMB control number.
PLEASE DO NOT RETURN YOUR FORM TO THE ABOVE ADDRESS.

1. REPORT DATE *(DD-MM-YYYY)* September 2012	**2. REPORT TYPE** Final	**3. DATES COVERED (From - To)**
4. TITLE AND SUBTITLE Surface Characteristics of Etched and Non-etched Silicon Germanium (SiGe)/Si Graded Structure with Varying Ge Concentration Grown by Ultra-high Vacuum (UHV)/Chemical Vapor Deposition (CVD) for Optoelectronic and Power Conversion Applications		**5a. CONTRACT NUMBER** **5b. GRANT NUMBER** **5c. PROGRAM ELEMENT NUMBER**
6. AUTHOR(S) Fred Semendy, Patrick Taylor, Greg Meissner, and Priyalal Wijewarnasuriya		**5d. PROJECT NUMBER** **5e. TASK NUMBER** **5f. WORK UNIT NUMBER**
7. PERFORMING ORGANIZATION NAME(S) AND ADDRESS(ES) U.S. Army Research Laboratory Attn: RDRL-SEE-I 2800 Powder Mill Road Adelphi, MD 20783-1197		**8. PERFORMING ORGANIZATION REPORT NUMBER** ARL-TR-6128
9. SPONSORING/MONITORING AGENCY NAME(S) AND ADDRESS(ES)		**10. SPONSOR/MONITOR'S ACRONYM(S)** **11. SPONSOR/MONITOR'S REPORT NUMBER(S)**

12. DISTRIBUTION/AVAILABILITY STATEMENT

Approved for public release; distribution unlimited.

13. SUPPLEMENTARY NOTES

14. ABSTRACT

Graded high-quality silicon germanium (SiGe) epitaxial layers were grown on n-type Si with varying Ge concentration using low-temperature ultra-high vacuum (UHV)/chemical vapor deposition (CVD). The graded layers were grown on Si substrates followed by a final growth of doped $Si_{1-x}Ge_x$ with varying percentage of Ge for comparison study. Various techniques, including atomic force microscopy (AFM), optical reflectance, and transmission were used to characterize the surface and structural quality of the materials. The investigation also included for the first time the reflectivity and absorbance of etched black silicon-germanium ($Si_{1-x}Ge_x$). Black $Si_{1-x}Ge_x$ was produced by metal enhanced chemical etching using nanometer-scale gold particles as the catalyst and hydrogen fluoride (HF):hydrogen peroxide (H_2O_2):acetic acid (CH_3COOH) as the etchant. The etched surface was black and textured, and showed strong suppression of reflectivity and enhanced absorption in the near-infrared, which are consistent with $Si_{1-x}Ge_x$ becoming highly surface-textured due to metal catalysis and wet etching. Lowering reflection and enhancing absorption in $Si_{1-x}Ge_x$ is an important milestone towards practical, extended wavelength (~2 µm) electro-optical applications. There is good evidence that varying Ge concentration affects the surface properties across different techniques in determining layer composition and thickness. The surface root-mean-square roughness before etching measured by AFM for all the samples indicate very smooth surfaces.

15. SUBJECT TERMS

SiGe/Ge, etched, UHV/CUD, black SiGe/Si, surface properties

16. SECURITY CLASSIFICATION OF:			**17. LIMITATION OF ABSTRACT**	**18. NUMBER OF PAGES**	**19a. NAME OF RESPONSIBLE PERSON**
a. REPORT	**b. ABSTRACT**	**c. THIS PAGE**			Fred Semendy
Unclassified	Unclassified	Unclassified	SAR	24	**19b. TELEPHONE NUMBER** (*Include area code*) (301) 394-4627

Standard Form 298 (Rev. 8/98)
Prescribed by ANSI Std. Z39.18

Contents

List of Figures **iv**

Acknowledgments **v**

1. Introduction **1**

2. Experiment **3**

3. Results and Discussion **5**

4. Conclusion **10**

5. References **11**

List of Symbols, Abbreviations, and Acronyms **13**

Distribution List **15**

List of Figures

Figure 1. Epitaxial SiGe layers on Si (001) with a pseudomorphic layer on the left and a partially relaxed layer on the right. 2

Figure 2. (a) Structure of the grown material, (b) 12% GeSi on graded GeSi on the Si substrate, (c) 30% GeSi on graded GeSi on the Si substrate, and (d) 40% GeSi on graded GeSi on the Si substrate with all layers n+ doped. 4

Figure 3. Experimental procedure for the nano catalyst formation on the SiGe surface. 5

Figure 4. Nomarski images of the surfaces of three very thick p-type samples: (a) 15% Ge, (b) 30% Ge, and (c) 50% Ge at 50×. 6

Figure 5. Normaski images of the surfaces of three n-type samples: (a) 12% Ge, (b) 30% Ge, and (c) 40% Ge at 50×. 7

Figure 6. AFM images of the surfaces of three samples: (a) 12% Ge, (b) 30% Ge, and (c) 40% Ge. 7

Figure 7. The step height from AFM images of the surfaces of three samples: (a) 12% Ge, (b) 30% Ge, and (c) 40% Ge. 8

Figure 8. Etch rate of $Si_{1-x}Ge_x$ in $HF:H_2O_2:CH_3COOH$ (1:2:3). 8

Figure 9. %R of unetched and etched samples: (a) Si0.85Ge0.15, (b) Si0.70Ge0.30, and (c) Si0.50Ge0.50. 9

Figure 10. The surface texture pattern of the sample $Si_{0.70}Ge_{0.30}$. 10

Acknowledgments

We would like to thank Dr. Mayank Bulsara at the Dept. of Materials Science and Engineering at the Massachusetts Institute of Technology for providing the high-quality black silicon-germanium ($Si_{(x)}Ge_{(1-x)}$) heteroepitaxial layers for this work.

INTENTIONALLY LEFT BLANK.

1. Introduction

Bandgap engineering with the well-established silicon (Si) technology has generated interest in combing Si with silicon germanium (SiGe) alloys, which provides a technological promise of new electronic, optoelectronic, and power conversion efficient devices (*1*). In the past few years, attempts such as "blackening" the surface of $Si_{1-x}Ge_x$ by metal enhanced etching (MEE) have been made at the U.S. Army Research Laboratory (ARL) to improve the optical property of absorption beyond 1.4 µm, which may make it a useful material of choice for infrared (IR) detection compared to expensive indium gallium arsenide (InGaAs) (*2*).

Semiconductor heterostructures such as SiGe/Si greatly enhance the range of possible device configuration and open the door for new phenomena such as tunneling, tenability of absorption, real space-carrier transfer, two-dimensional (2-D) carrier gases, and quantum size effects. Over the past several years, advances in SiGe technology have shown impressive potential for the development of advanced Si-based electronic and optical devices, and thermoelectric generators incorporating Ge. In particular, SiGe heterostructure technology is beginning to rival III–V semiconductors in many applications (*3–5*). Heteroepitaxy is the epitaxial growth of multiple dissimilar materials to form a layered heterojunction (HJ). HJs can be used to drive both carriers in to the same volume; separate carriers from the parent dopant atoms; or form local accumulation or depletion regions independent of doping. This behavior contrasts sharply with homojunctions. HJ devices offer an immensely larger array of device configurations and has become the basis for the band gap engineering (*6*). However, HJ devices are very rare because the dominant semiconductor Si is not compatible with any other semiconductor. Therefore, heterojunction devices have been based mostly upon III-V, and II-VI compound semiconductors materials. However, these materials are very expensive with inferior thermal and mechanical properties, leading to lower crystalline perfection.

Heterostructures are based on differences in the electronic bandstructure of the component semiconductors. All of the common semiconductors are based on four fold tetragonally oriented bonds in a diamond like configuration. Adding any dopant from the III- or V- to Si can cause segregation (*7, 8*). This occurs because the condensing Si atom has a finite probability of exchanging positions with a surface dopant atom. Another problem is that Si-based heterostructures may not grow as flat layers. This is due to the size difference as well as the character of the bonds being covalent versus polar with respect Si, e.g., gallium phosphide (GaP) has a small lattice misfit with Si, but grows as three-dimensional (3-D) islands because of bonding differences. Hence GaP/Si grows as isolated 3-D islands (*9*). With a continuous effort, the islands will coalesce and form continuous layers. In general, such materials will be highly doped and usually with a thickness greater than 1 µm. Fortunately, Ge can be used for growing

misfit accommodated SiGe/Si heterostructures to form HJ devices: the natural column IV pairing of Si is with Ge. Ge has an atomic spacing of 4.2% larger than that of Si, so lattice misfit is one issue that needs to be managed to obtain low defect-density. To that end, in this work we pursue a special pseudomorphic growth mode to grow $Si_{(x)}Ge_{(1-x)}$ alloys on Si with low defect density

Figure 1 gives a depiction of the pseudomorphic layer on the left and a partially relaxed layer on the right.

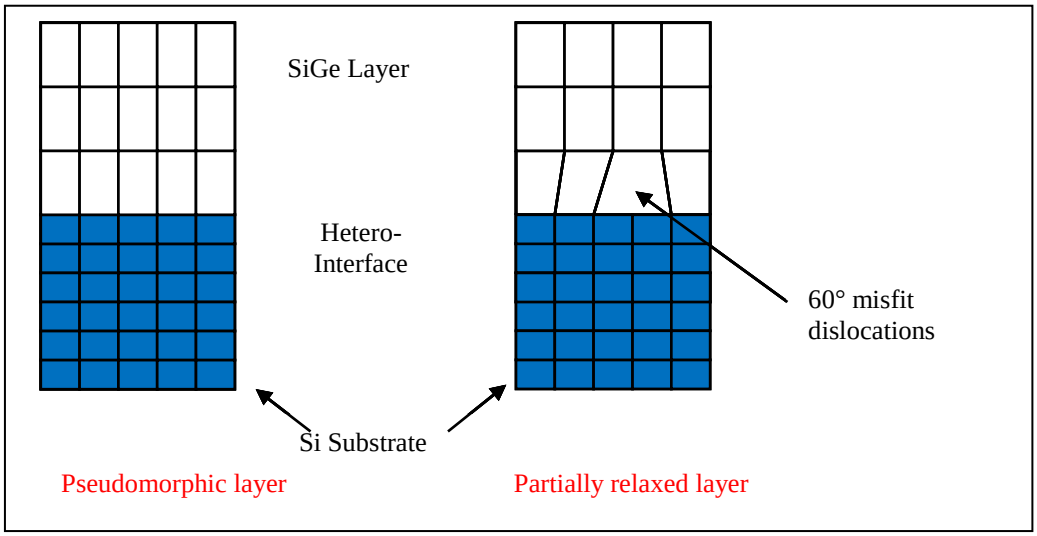

Figure 1. Epitaxial SiGe layers on Si (001) with a pseudomorphic layer on the left and a partially relaxed layer on the right.

A SiGe layer pseudomorphically grown on a Si substrate is elastically strained. The in-plane lattice parameter is equal to that of Si, and thus, is smaller than the lattice parameter of the bulk SiGe layer. Likewise, the out-of-plane lattice constant is larger than that of the bulk SiGe alloy. When the film thickness exceeds the critical thickness for pseudomorphic growth, the mismatch strain is relieved by the formation of misfit dislocations—as shown in figure 1 on the right side. At low mismatch strain, $Si_{1-x}Ge_x$ /Si (001) structures relax by the introduction of 60° dislocations. Hence, the goal for fabricating good quality reliable devices is to use a defect-free device structure on the substrate.

Many attempts have been made in growing defect-free structures by introducing compositional grading (*10, 11*) and low-temperature buffer layers (*12, 13*). These two techniques are highly successful leading to reductions in density of threading dislocations by 4–5 orders of magnitude. However, irrespective of these methods to reduce dislocations, strain relaxation results in an undulation in the surface morphology (*14*) known as "crosshatch" pattern (*15*). The crosshatch is characteristic of low misfit regime—with a lattice mismatch less than 2%. It has been observed in almost all heterostructures. The crosshatch-related surface roughening can affect

carrier mobility and the quality of quantum structures grown on such surfaces. It is not compatible with planar integrated circuit technologies, the major driver for applications.

To eliminate the defects, it is therefore very important to understand their structure and origin. Atomic force microscopy (AFM) and transmission electron microscopy (TEM) techniques are used to study evolution of surface morphology during strain relaxation and the mechanism by which dislocations give rise to crosshatching. Two types of models have been proposed (*16*). In the first model, the formation of crosshatch patterns is caused by surface diffusion during growth in response to the inhomogeneous strain fields arising from the network of misfit dislocations. The second model suggests that crosshatching results from the surface steps at the intersection of the epilayer surface and the misfit dislocation glide plane, and is a result of plastic shear displacements (*17*). The two mechanisms are, in fact, not mutually exclusive. Therefore, along the path towards demonstration of a successful etched SiGe IR absorber layer, we report the results of a combined AFM and Nomarski microscope images of the SiGe layers with special focus on understanding crosshatching, because of the importance that crosshatching can play in producing high-performance devices. Next along that path, we employ optical reflectance and transmission to study the blackened $Si_{1-x}Ge_x$/Si materials.

Increased absorption of light is essential to create highly efficient photovoltaic devices. To achieve this, efficient 3-D structures with relevant material systems are required. Apart from these two techniques, others (*18, 19*) have proposed a technique in which multicrystalline SiGe bulk crystal with microscopic compositional distribution is grown using the casting technique. The average Ge composition was changed systematically between 0% and 10%. A small addition of Ge to multicrystalline Si was found to be very effective to increase the short-circuit current density without affecting the open-circuit voltage. They also indicated that such grown SiGe materials are promising candidates for solar cell and other optoelectronic applications. For such applications, SiGe has to be prepared with reduced reflectivity and increased absorbance. This can be achieved through surface texturing, as has been used in the case of black Si. In general, for a 3-D blackened surface, reactive ion etching or wet anisotropic etching are the techniques of choice. Although reactive ion etching can provide a structure with a high aspect ratio, it involves rather complicated procedures. MEE (*20, 21*), by which Si is etched using metal thin films or particle as catalysts, is an attractive procedure because it is simple and easier to perform with good results.

2. Experiment

The $Si_{(x)}Ge_{(1-x)}$ alloy layers in this work were grown on 8-in Si substrates having either (111) or (100) orientation. The unusual growth method was accomplished using a special ultra-high

vacuum (UHV)/chemical vapor deposition (CVD) reactor, which proceeds by decomposition of gas-phase Si (silane) and Ge (germane) compounds to deposit the $Si_{(x)}Ge_{(1-x)}$ alloys of interest. Because there is a large lattice misfit between pure Si and the $Si_{(x)}Ge_{(1-x)}$ alloy layers, a strategy to minimize lattice defects was that employs a graded lattice parameter that starts at a pure Si buffer layer and ends at the alloy of interest. Three planar $Si_{(x)}Ge_{(1-x)}$ alloys were prepared: $Si_{60}Ge_{40}$, $Si_{70}Ge_{30}$, and $Si_{88}Ge_{12}$. The substrates and all layers were intentionally doped n-type. The thickness of the layers differed slightly because the end-point alloy was different in each case. For the $Si_{60}Ge_{40}$ layer, the total thickness was 0.5 µm; for the $Si_{70}Ge_{30}$, the total thickness was 0.4 µm; and lastly for the $Si_{88}Ge_{12}$, the total thickness was 0.25 µm.

Using such a large thickness assures that although some small residual strain probably exists after growth, the large misfit strain is mostly relaxed through the introduction of dislocations. However the graded lattice parameter approach minimizes that and yields device-quality material. In order to avoid strain-induced surface undulations in such highly compressively strained layers, the $Si_{(x)}Ge_{(1-x)}$ alloy layers were grown at 350–400 °C. Although UHV-CVD growth allows highly perfect crystalline quality with little impurity incorporation even with growth rates as low as 10^{-3}Å/s, the intentional doping was targeted to $2x10^{18}/cm^3$ donors, which causes ionized impurity scattering of carriers. There was some variation in the measured Hall mobility, but the range was always <1000cm^2/V-s because of alloy-scattering, and scattering from dislocations and ionized impurities.

Figure 2 gives the structure of the material grown with varying Ge concentration. Figure 2a is the depiction of the structure with growth of graded layers on an Si substrate with top layer of GeSi with varying Ge. The graded region thickness varies as one go from 12 % Ge in the first sample to the third sample 40%.

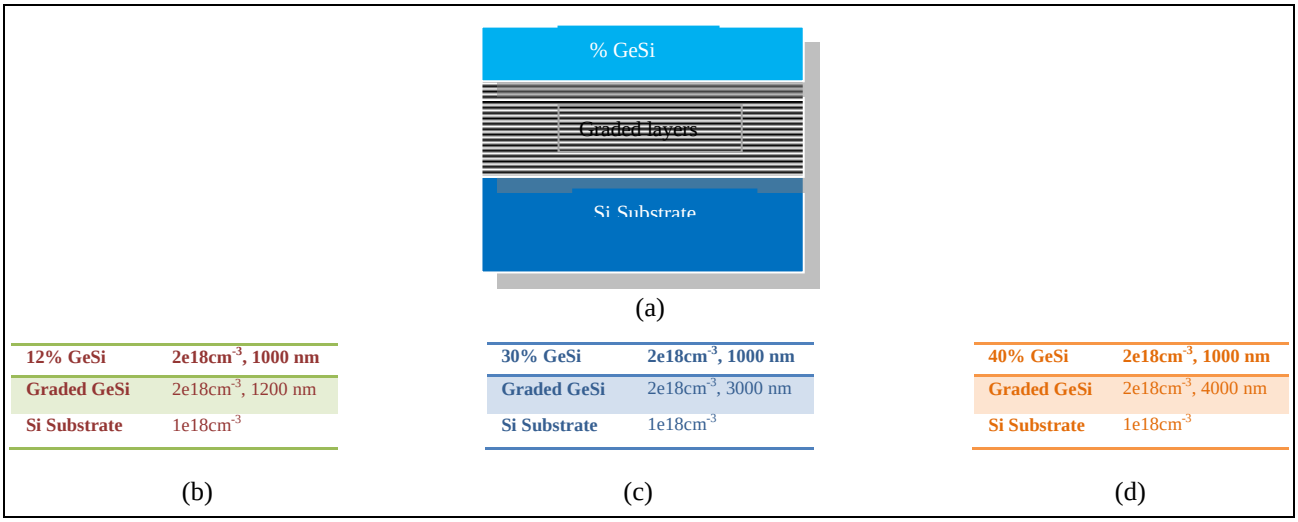

Figure 2. (a) Structure of the grown material, (b) 12% GeSi on graded GeSi on the Si substrate, (c) 30% GeSi on graded GeSi on the Si substrate, and (d) 40% GeSi on graded GeSi on the Si substrate with all layers n+ doped.

The samples were inspected using AFM to make sure nanoparticles of gold (Au) are randomly oriented on the surface of $Si_{1-x}Ge_x$. In the next part of the experiment, a set of samples without Au were etched in solution of hydrogen fluoride (HF):hydrogen peroxide (H_2O_2):acetic acid (CH_3COOH) (1:2:3). Care was taken to wait 30 min prior to using this etchant. The etching of the samples in the above solution showed linearity in the etch rate and proceeded to darkened surface. Once the etch rate was determined for different compositions of $Si_{1-x}Ge_x$, etching was carried out with a newly prepared solution of HF: H_2O_2: CH_3COOH (1:2:3). After etching in that solution as part of the texturing process, the samples were thoroughly cleaned and blow dried with nitrogen. The solution etched $Si_{1-x}Ge_x$ while slowly preserving the surface polish. However, etching the samples for more than 10 min showed visible damage. Finally, the etched samples were dipped in an aqueous solution of iodine (I) and potassium iodide (KI) (25 gm I and 100 gm KI per liter of water [H_2O]) (*22*). The samples were further cleaned in running de-ionized water and dried with nitrogen. These samples were further used for AFM surface analysis and optical reflection and transmission measurements using a Perkin Elmer 950 ultraviolet (UV)-visible-near IR spectrometer. These steps are shown in figure 3.

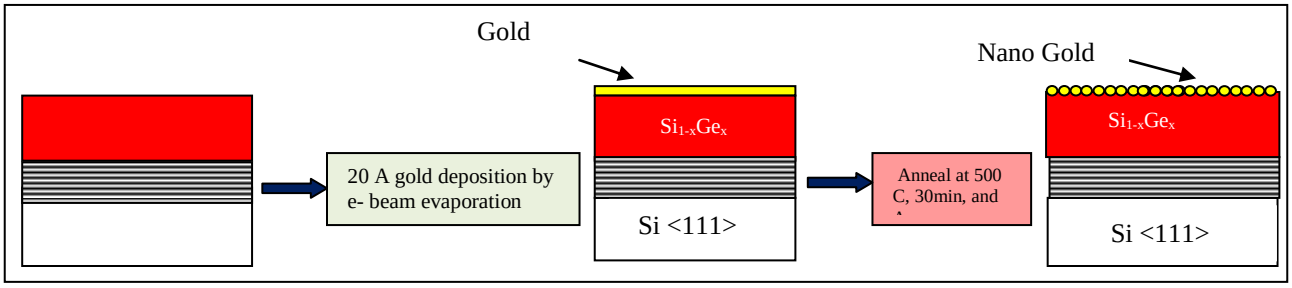

Figure 3. Experimental procedure for the nano catalyst formation on the SiGe surface.

3. Results and Discussion

SiGe/Si samples with varying Ge were cleaned using standard procedures and surface of a number of samples were characterized using AFM and a Nomarski microscope. AFM is analogous to a surface profiler, where a sharp tip is dragged over the sample, and the movement of the tip is monitored as a measure of sample topography. Differential interference contrast microscopy (DIC), also known as Nomarski Interference Contrast (NIC) or the Nomarski microscopy, is an optical microscopy illumination technique used to enhance the contrast in unstained, transparent samples. DIC works on the principle of interferometry to gain information about the optical path length of the sample and see otherwise invisible features. A relatively complex lighting scheme produces an image with the object appearing black to white on a grey background. This image is similar to that obtained by phase contrast microscopy but

without the bright diffraction halo. DIC works by separating a polarized light source into two orthogonally polarized mutually coherent parts which are spatially displaced (sheared) at the sample plane, and recombined before observation. The interference of the two parts at recombination is sensitive to their optical path difference (i.e., the product of refractive index and geometric path length). Adding an adjustable offset phase determining the interference at zero optical path difference in the sample, the contrast is proportional to the path length gradient along the shear direction, giving the appearance of a 3-D physical relief corresponding to the variation of optical density of the sample, emphasizing lines and edges though not providing a topographically accurate image. Figure 4 shows the Nomarski images of the surfaces of three samples.

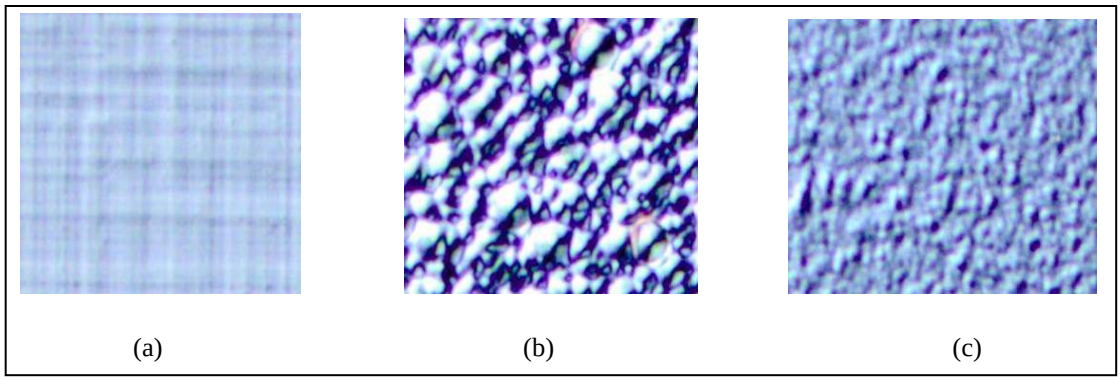

Figure 4. Nomarski images of the surfaces of three very thick p-type samples: (a) 15% Ge, (b) 30% Ge, and (c) 50% Ge at 50×.

As shown in figure 4, sample (a) with 15% Ge clearly shows the crosshatch pattern. However, (b) and (c) indicate the 3-D island structuring. Despite the fact that the $Si_{(x)}Ge_{(1-x)}$ alloys are very similar, the reason 3-D growth is observed in the layers of figure 4 and not in figure 5 is that a graded layer is used for the layers in figure 5, and the layers of figure 4 are grown without grading. Figure 5 depicts the Nomarski pictures of the three graded samples with (a) 12% Ge, (b) 30% Ge, and (c) 40% Ge in the SiGe/Si structure The crosshatch pattern is evident in all three better-grown samples and it appears that the pattern enlarges for higher concentration of Ge.

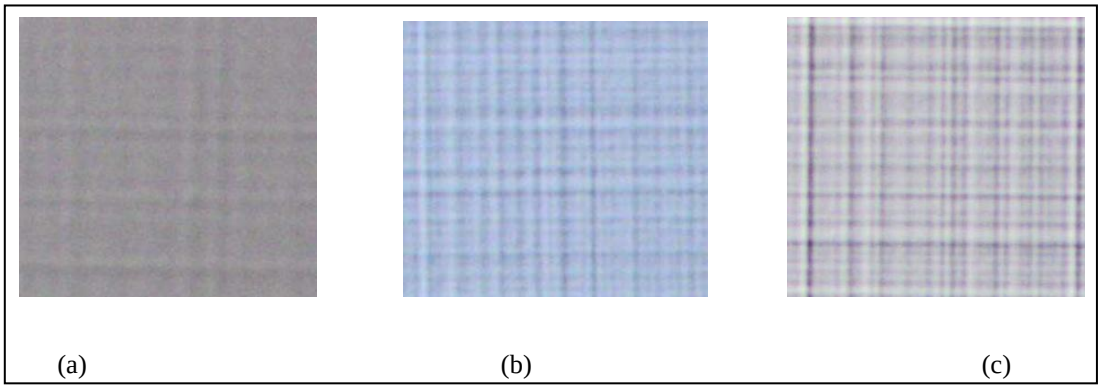

Figure 5. Normaski images of the surfaces of three n-type samples: (a) 12% Ge, (b) 30% Ge, and (c) 40% Ge at 50×.

The high concentration is evident in the AFM scan of the same samples, as shown in figure 6. The root mean square (rms) values were 1.22 nm, 3.29 nm, and 7.37 nm for samples (a), (b), and (c), respectively, indicating that the rms value doubles as one increases the concentration of Ge.

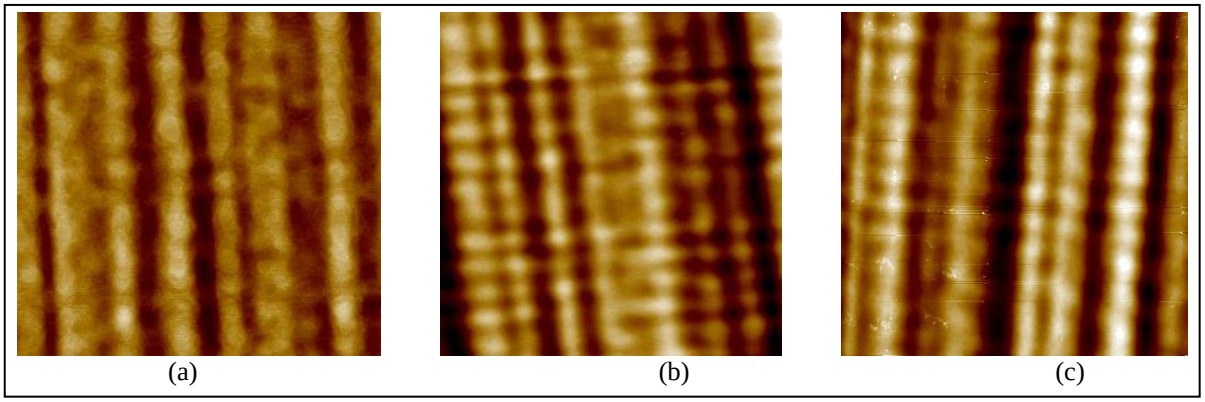

Figure 6. AFM images of the surfaces of three samples: (a) 12% Ge, (b) 30% Ge, and (c) 40% Ge.

Figure 7 shows increasing step height and width of steps of the samples as the amount of Ge is increased from sample to sample, showing a peak-to-peak difference in the crosshatch as well as indirectly depicting the increase of the rms values as the amount of Ge increases. AFM clearly provides a good measure of the nature of the surface as the amount of Ge is increased from sample to sample.

Some of the samples were thinned by lapping and polishing using a Logitech Lapping System. Here the goal was to make sure that the samples under consideration were double-side polished to reduce Rayleigh scattering during the pass-through of the IR light probe. Samples were cleaned and 20 Å of Au was deposited on the $Si_{1-x}Ge_x$ surface using an e-beam evaporator, which was kept at a pressure lower than $1x10^{-6}$ mTorr. Small pieces of these samples with appropriate masking were etched with $HF:H_2O_2:CH_3COOH$ (1:2:3). The etching solution was freshly prepared and left at room temperature for 30 min for stabilization before use. Etching

was done at room temperature (25 °C) in polypropylene beakers with slight agitation. The samples were 1 cm^2 in area in area in ~100 ml of fresh solution of $HF:H_2O_2:CH_3COOH$ (1:2:3). Figure 8 shows the etching depth with respect to time of $Si_{1-x}Ge_x$ (with varying x values) in $HF:H_2O_2:CH_3COOH$ (1:2:3).

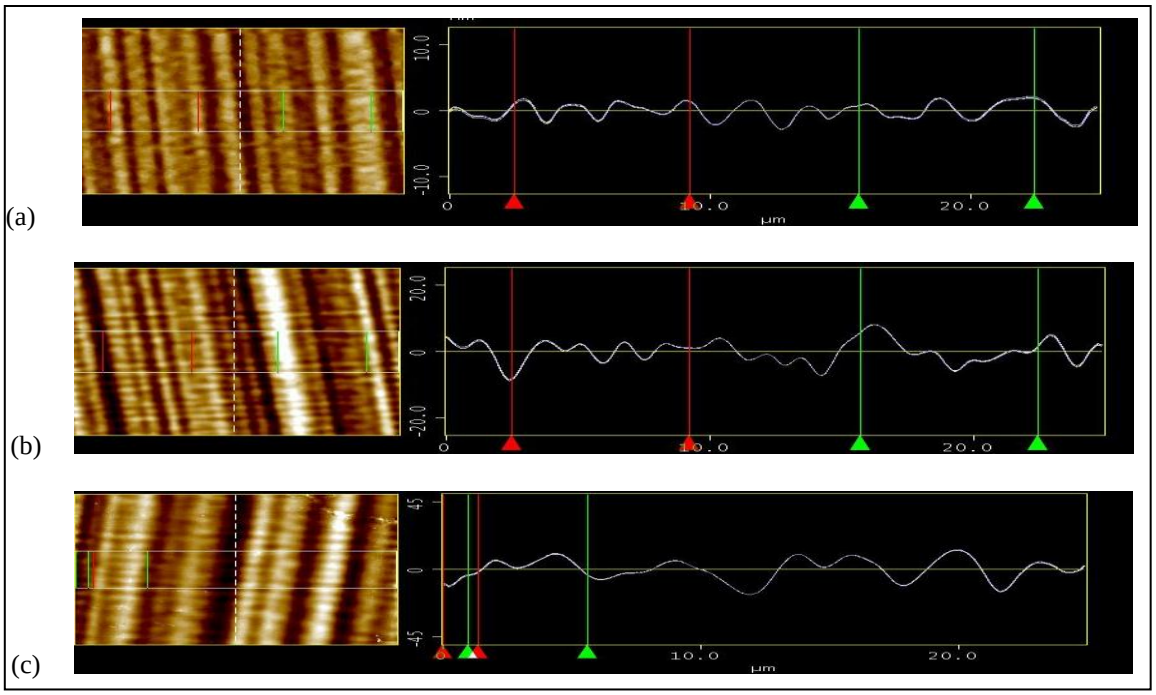

Figure 7. The step height from AFM images of the surfaces of three samples: (a) 12% Ge, (b) 30% Ge, and (c) 40% Ge.

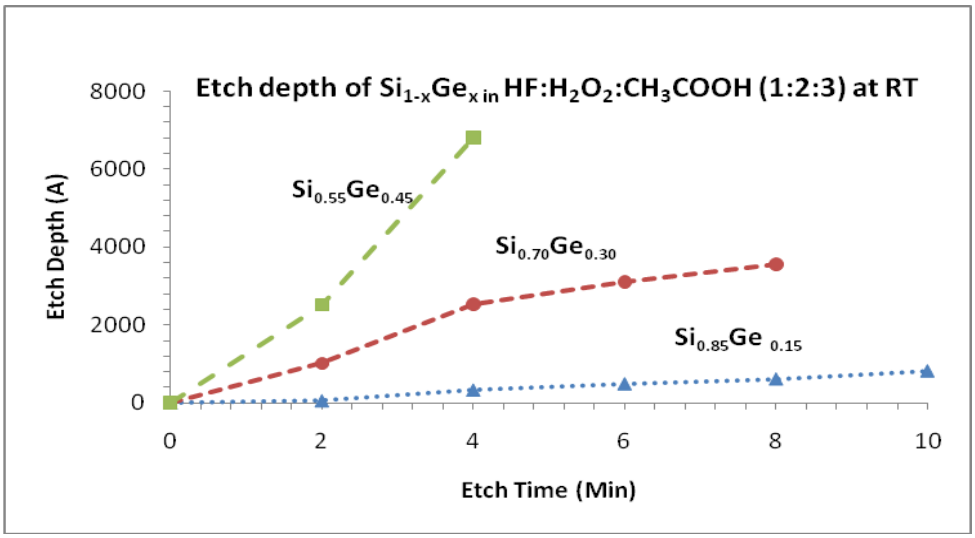

Figure 8. Etch rate of $Si_{1-x}Ge_x$ in $HF:H_2O_2:CH_3COOH$ (1:2:3).

The linear etching behavior is clearly evident from the Ge concentration in the $Si_{1-x}Ge_x$. The rapid increase in etch rate can be explained by the presence of an increased number of Ge surface atoms. The bonding energy reveals the difficulty in breaking the Si-Si bonds, which is 78 kcal/mol; the Ge-Si bond dissociation energy is 72 kcal/mol and the Ge-Ge bond dissociation energy is 65 kcal/mol (*23*). The more Ge-Ge and Ge-Si bonds are exposed, the higher the etching rate is, as can be seen from the graph. The etched surface provided a greyish blackened surface. The etch rate was found to be less than 100 Å for $Si_{0.85}Ge_{0.15}$, about 500 Å for $Si_{0.70}Ge_{0.30}$ and about 1300 for $Si_{0.55}$ $Ge_{0.45}$.

Optical measurements were performed as follows. After measuring the %T and %R, we used the equation, A = 1 – T – R, to obtain the absorbance. Unetched, etched, and thinned samples were used for the measurement of %T and %R, which we then applied to the above formula to calculate the percent absorbance. The results etched and unetched samples are plotted in figure 9. The spectrum shows the reflectivity behavior of a thin film with a thickness of ~1.6 µm of the $Si_{1-x}Ge_x$ layer on the Si (111) substrate. The spectrum shows considerable reduction in reflectivity for $Si_{1-x}Ge_x$ samples after etching, as can be seen.

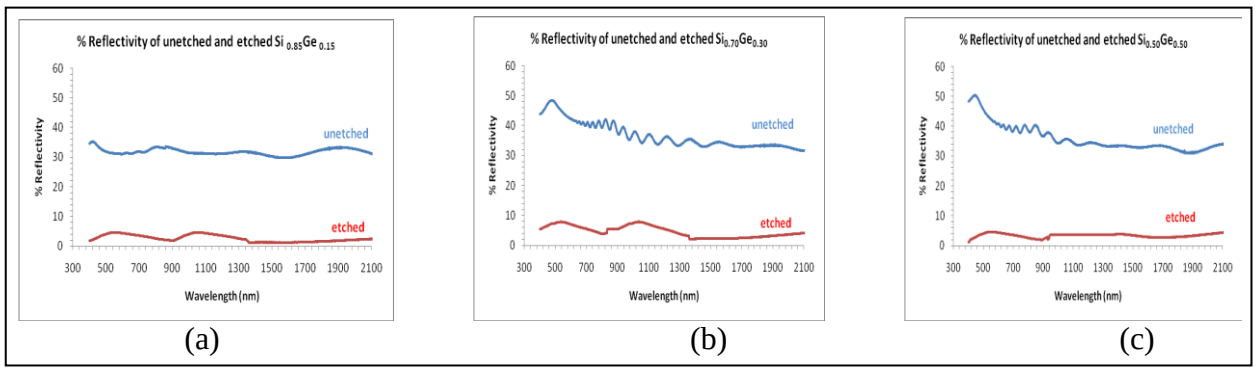

Figure 9. %R of unetched and etched samples: (a) Si0.85Ge0.15, (b) Si0.70Ge0.30, and (c) Si0.50Ge0.50.

As can be seen from the plots, the reflectivity goes through substantial reduction after the etching. The reflectivity reduces by ~85% for samples by MEE especially in the IR region. This lowering of reflectivity definitely indicates surface modification with micro-structure formation due to the wet etch processing. The etched samples were further characterized using a Veeco surface topography profiler. The system's white light interferometry can measure surface topography from nanometer-scale roughness through millimeter-scale steps with sub-nanometer resolution. This surface metrology system was used to understand the surface texture patterns and parameters of the etched surface. Figure 10 gives the surface texture pattern of the sample $Si_{0.70}Ge_{0.30}$. The curves on the right indicate the *x*-axis (red) and *y*-axis (blue), as shown on the middle cross wire.

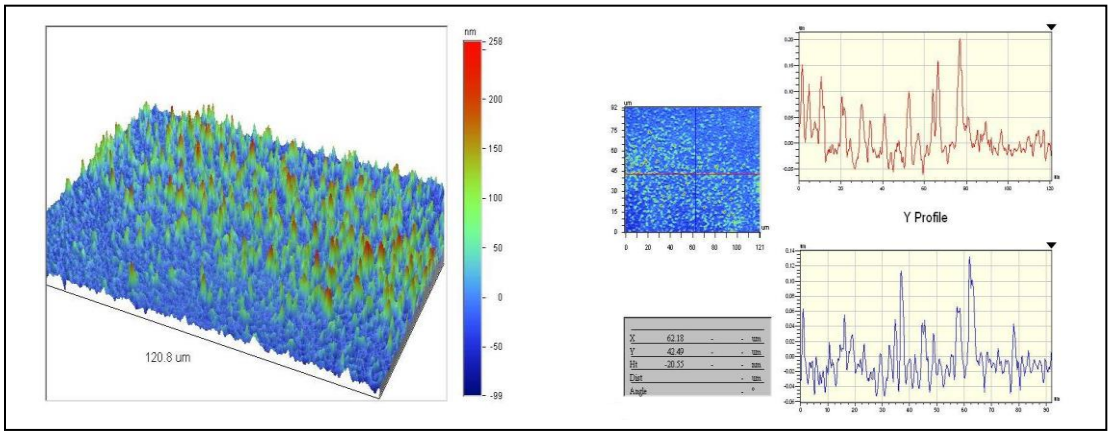

Figure 10. The surface texture pattern of the sample $Si_{0.70}Ge_{0.30}$.

4. Conclusion

We reported here, for the first time, an investigation of surface and optical properties of reflection and transmission of compositional $Si_{1-x}Ge_x$ semiconductor alloys after treating them with metal enhanced chemical etching using nano-sized Au particles as the catalyst and $HF:H_2O_2:CH_3COOH$ as the etchant. The etched surface became black and textured, and showed a suppression of reflectivity and an enhancement of absorption in the near-IR region. Conceivably, the black $Si_{1-x}Ge_x$ became micro-structured due to the metal catalysis and wet etching. Surface texturing was visible, as shown by the plots, and became extreme in the case of $Si_{0.55}Ge_{0.45}$. Visible separation in the *x-y* plots positively indicates this behavior, which is due to the lower amount of Si and an excess amount of Ge in $Si_{1-x}Ge_x$. Through this work, we have shown that $Si_{1-x}Ge_x$ can be made black using metal enhanced chemical etching. We have also shown that such black $Si_{1-x}Ge_x$ has reduced reflectivity and enhanced absorbance in the near-IR region.

Detectors made with this type of black $Si_{1-x}Ge_x$ will have higher performance in the extended IR region. This lowering of reflection and enhancement of absorption may have important practical implications for making efficient photovoltaic and photodetecting applications using compositional $Si_{1-x}Ge_x$ alloys. Currently, we are fabricating photodetectors to prove our conclusion.

5. References

1. Cressler, J. D. *IEEE Spectrum* **1995**, *32*, 49.
2. Semendy, F.; Taylor, P.; Meissner, G.; Wijewarnasuriya, P. *Black SiGe for Extended Wavelength Near Infrared Electro-optical Applications*; ARL-TR-5202: U.S. Army Research Laboratory: Adelphi, MD, 2010.
3. Voinigescu, S.; Schumacher, M.; Ineswski, K.; Lisak, R.; Parpia, Z. *Electromn Technology* **1993**, *26* (4), 25–64, Institute of Electron Technology, Warszawa.
4. Lee, M.; Fitzgerald, E.; Bulsara, M.; Currie, M.; Locktefield, A. *J. Appl. Phys* **2005**, *97*, 011101.
5. Shirukai, Y.; Sakai, A. *Sur. Sci, Reports* **2005**, *59*, 153–207.
6. Cappaso, F. *J. Vac. Sci. Technol* **1983**, *B1*, 457–461.
7. Becker, G. E.; Bean, J. C. *Appl. Phys* **1977**, *48*, 4395–3399.
8. Bean, J. C. *Appl. Phys. Lett.* **1978**, *33*, 654–656.
9. Gonda, S.; Matushima, Y.; Mukai, S.; Makita, Y.; Igarashi, O. *Jap. J. Appl. Phys* **1978**, *17*, 1043–1048.
10. Fitzgerald, E. A.; Xie, Y.-H. I.; Green, M. L.; Brasen, D.; Kortan, A. R.; Michel, J.; Mii, Y.-J; Weirv, B. E. *Appl. Phys. Lett* **1991**, *59*, 811.
11. LeGoues, F. K.; Meterson, B. S.; Morar, J. F. *Phys. Rev. Lett.* **1991**, *66*, 2903.
12. LeGoues, F. K.; Rosenberg, R.; Meterson, B. S. *Appl. Phys. Lett* **1989**, *54*, 644.
13. Papagno, L.; Frankel, D.; Chen, Y.; Caputi, L. S.; Anderson. J.; Lapeyre, G. J. *Surf. Sci.* **1991**, *248*, 343.
14. Eugene, J.; Legoues, T. K.; Kesan, V. P.; Iyer, S. S.; d'Heurle, F. M. *Appl. Phys. Lett* **1991**, *59*, 78.
15. Kishino, S.; Ogirima, M.; Kurata, K. *J. Electrochem. Soc* **1972**, *119*, 617.
16. Shiryaev, S. Yu.; Jensen, F.; Peterson, J. W. *Appl. Phys. Lett* **1994**, *64*, 3305.
17. Hammond, R.; Phillips, P. J.; Whall, T. E.; Parker, E.H.C.; Graf, T.; Von Känel, H.; Shields A. J. *Appl. Phys. Lett* **1979**, *71*, 2517.

18. Koynov, S.; Brandt, M. S.; Stutzmann, M. *Appl. Phys. Lett* **2006**, *88*, 203107.

19. Wu, C.; Crouch, C. H.; Zhao, L.; Carey, J. E.; Yonkin, R.; Levinson, J. A.; Mazur, E.; Farell, R. M.; Gothoskar, P.; Karger, A. *Appl. Phys. Lett* **2001**, *73*, 1850.

20. Nakajima, K.; Usami, N.; Fujiwara, K.; Murakami, Y.; Ujihara, T.; Sazaki, G.; Shishido, T. *Sol. Energy Mater. Sol. Cells* **2002**, *93*, 72.

21. Nakajima, K.; Usami, N.; Fujiwara, K.; Murakami, Y.; Ujihara, T.; Sazaki, G.; Shishido, T. *Sol. Energy Mater. Sol. Cells* **2002**, *93*, 305.

22. Li, X.; Boh, P. W. *Appl. Phys. Lett* **2000**, *77*, 2572.

23. Yee, S.; Kawamoto, Y.; Tanaka, H.; Fukumuro, N.; Matsuda, H. *Elechem. Comm.* **2003**, *5*, 632.

List of Symbols, Abbreviations, and Acronyms

2-D	two-dimensional
3-D	three-dimensional
AFM	atomic force microscopy
ARL	U.S. Army Research Laboratory
Au	gold
CH_3COOH	acetic acid
CVD	chemical vapor deposition
DIC	differential interference contrast
GaP	gallium phosphide
Ge	germanium
H_2O	water
H_2O_2	hydrogen peroxide
HF	hydrogen fluoride
HJ	heterojunction
I	iodine
InGaAs	indium gallium arsenide
IR	infrared
KI	potassium iodide
MEE	metal enhanced etching
NIC	Nomarski Interference Contrast
RMS	root mean square
Si	silicon
SiGe	silicon germanium

TEM	transmission electron microscopy
UHV	ultra-high vacuum
UV	ultraviolet

NO. OF COPIES	ORGANIZATION
1 ELEC	ADMNSTR DEFNS TECHL INFO CTR ATTN DTIC OCP 8725 JOHN J KINGMAN RD STE 0944 FT BELVOIR VA 22060-6218
1	DARPA MTO ATTN N DHAR 3701 NORTH FAIRFAX DR ARLINGTON VA 22203-1714
1	US ARMY RSRCH DEV AND ENGRG CMND ARMAMENT RSRCH DEV & ENGRG CTR ARMAMENT ENGRG & TECHNLGY CTR ATTN AMSRD AAR AEF T J MATTS BLDG 305 ABERDEEN PROVING GROUND MD 21005-5001
1	ARMY RESEARCH OFFICE ATTN RDRL ROE L W CLARK III PO BOX 12211 RESEARCH TTRIANGLE PARK NC 27709
2	CECOM NVESD ATTN AMSEL RD NV A SCHOLTZ ATTN AMSEL RD NV D BENSON 10221 BURBECK RD STE 430 FT BELVOIR VA 22060-5806
1	CM ACOUSTIC AND NETWORKED SENSORS DIV ATTN V SWAMINATHAN PICATINNY NJ 07806-5000
1	US ARMY ARDEC-BENET LABS ATTN J WARRENDER WATERVLIET ARSENAL NY 12189
1	US ARMY INFO SYS ENGRG CMND ATTN AMSEL IE TD A RIVERA FT HUACHUCA AZ 85613-5300

NO. OF COPIES	ORGANIZATION
1	US GOVERNMENT PRINT OFF DEPOSITORY RECEIVING SECTION ATTN MAIL STOP IDAD J TATE 732 NORTH CAPITOL ST NW WASHINGTON DC 20402
1	DIRECTORATE FOR ENGRG ECCS DIV NATIONAL SCIENCE FOUNDATION ATTN A B KAUL 4201 WILSON BLVD, RM 525 ARLINGTON VA 22230
1	GENERAL TECHNICAL SERVICES ATTN G P MEISSNER 3100 ROUTE 138 WALL NJ 07719
62	US ARMY RSRCH LAB ATTN IMAL HRA MAIL & RECORDS MGMT ATTN RDRL CI J PELLEGRINO ATTN RDRL CIO LL TECHL LIB ATTN RDRL CIO LT TECHL PUB ATTN RDRL SE T BOWER ATTN RDRL SED E B MORGAN ATTN RDRL SED E K A JONES ATTN RDRL SED E M LITZ ATTN RDRL SED P A LELIS ATTN RDRL SEE E N GUPTA ATTN RDRL SEE E R TOBER ATTN RDRL SEE G WOOD ATTN RDRL SEE I B ZANDI ATTN RDRL SEE I D BEEKMAN ATTN RDRL SEE I F SEMENDY (12 COPIES) ATTN RDRL SEE I G BRILL ATTN RDRL SEE I J LITTLE ATTN RDRL SEE I K K CHOI ATTN RDRL SEE I K OLVER ATTN RDRL SEE I P FOLKES ATTN RDRL SEE I P TAYLOR ATTN RDRL SEE I P UPPAL ATTN RDRL SEE I S SVENSSON ATTN RDRL SEE I S TRIVEDI ATTN RDRL SEE I W BECK ATTN RDRL SEE I W SARNEY ATTN RDRL SEE I Y CHEN

ATTN RDRL SEE L BLISS
ATTN RDRL SEE M G DANG
ATTN RDRL SEE M
G GARRETT
ATTN RDRL SEE M M REED
ATTN RDRL SEE M
M TAYSING-LARA
ATTN RDRL SEE M
M WRABACK
ATTN RDRL SEE M
N BAMBHA
ATTN RDRL SEE M N DAS
ATTN RDRL SEE M P SHEN
ATTN RDRL SEE M W CHANG
ATTN RDRL SEE O N FELL
ATTN RDRL SEE O
P PELLEGRINO
ATTN RDRL SEE P GILLESPIE
ATTN RDRL SEG N MARK
ATTN RDRL SER E
A DARWISH
ATTN RDRL SER E P SHAH
ATTN RDRL SER L
A WICKENDEN
ATTN RDRL SER L B NICHOLS
ATTN RDRL SER L E ZAKAR
ATTN RDRL SER L M DUBEY
ATTN RDRL SER L M ERVIN
ATTN RDRL SER L
S KILPATRICK
ATTN RDRL SER
P AMIRTHARAJ
ATTN RDRLL-SEE-I
K S RAMSEY
ADELPHI MD 20783-1197